Assessment of Severity of Coronary Artery Stenosis in a Canine Model Using the PET Agent ^{18}F-Fluorobenzyl Triphenyl Phosphonium: Comparison with ^{99m}Tc-Tetrofosmin

Igal Madar[1], Hayden Ravert[1], Antony DiPaula[2], Yong Du[1], Robert F. Dannals[1], and Lewis Becker[2]

[1]*Division of Nuclear Medicine, The Russell H. Morgan Department of Radiology, The Johns Hopkins Medical Institutions, Baltimore, Maryland; and* [2]*Department of Medicine, The Johns Hopkins Medical Institutions, Baltimore, Maryland*

Myocardial perfusion imaging plays an important role in clinical management of coronary artery disease, but the most commonly used radionuclides significantly underestimate the severity of coronary artery stenosis. The objective of this study was to evaluate the potential clinical utility of the PET compound ^{18}F-fluorobenzyl triphenyl phosphonium (^{18}F-FBnTP) and characterize its capacity to assess the severity of coronary artery stenosis in a canine model in vivo and ex vivo. **Methods:** ^{18}F-FBnTP myocardial uptake was measured in 17 dogs with various degrees of stenosis of the left anterior descending (LAD) or circumflex (LCx) coronary arteries during adenosine vasodilation, using dynamic PET and γ-well counting. True myocardial blood flow in ischemic (IS) and nonischemic (NIS) beds of the left ventricle was determined with radioactive microspheres. ^{18}F-FBnTP and ^{99m}Tc-tetrofosmin activities were compared in 8 dogs ex vivo. **Results:** The quantitative assessment of the perfusion defect was significantly ($P < 0.03$) more accurate with ^{18}F-FBnTP than with ^{99m}Tc-tetrofosmin, in mild (IS/NIS; 0.72 ± 0.08, 0.93 ± 0.07, respectively, mean ± SE) and severe stenosis (0.42 ± 0.05, 0.64 ± 0.08, respectively), compared with microsphere flow (mild, 0.43 ± 0.06; severe, 0.22 ± 0.04). The IS/NIS ratio of both radionuclides correlated linearly with microsphere flow disparity with a similar slope. Flow defect contrast was 2.7 times greater for ^{18}F-FBnTP than for ^{99m}Tc-tetrofosmin, as inferred from the regression line intercept (0.14 vs. 0.38, respectively). The ^{18}F-FBnTP PET IS/NIS ratio (mild, 0.70 ± 0.04; severe, 0.46 ± 0.02), did not differ statistically ($P \geq 0.330$) from that measured ex vivo. A nearly identical qualitative and quantitative estimate of stenosis severity was obtained by early, short (5–15-min) and delayed, prolonged (30–60-min) ^{18}F-FBnTP PET scans. The stenotic area measured by PET was 16% smaller than that defined by tissue staining. **Conclusion:** ^{18}F-FBnTP PET is a promising new technology for rapid noninvasive detection and assessment of perfusion defect severity in the myocardium.

Key Words: ischemia; perfusion; heart; PET; FBnTP; tetrofosmin

J Nucl Med 2007; 48:1021–1030
DOI: 10.2967/jnumed.106.038778

Myocardial perfusion SPECT is an excellent tool for risk stratification in coronary artery disease (CAD), thus effectively guiding decisions regarding revascularization (*1*). Currently, the SPECT radionuclide ^{201}Tl and the technetium complexes ^{99m}Tc-sestamibi and ^{99m}Tc-tetrofosmin are the mainstay of myocardial perfusion imaging (MPI) tests. SPECT MPI has relatively high sensitivity in detecting flow defect (averaged 87%) but lower specificity (averaged 75%) (*2*). Two important factors affect the accuracy of the diagnostic test: uncorrected nonuniform attenuation and photon scatter from extracardiac structures with relatively intense uptake, particularity the liver (*3,4*). Attenuation artifacts are frequent in 2 large groups of patients, women and obese subjects (*5*). Attenuation-compensation techniques in SPECT still leave room for improvement, when compared with PET, and may enhance photon scatter from liver (*6*). In some cases with fixed perfusion defect, electrocardiographically gated SPECT could help to discern attenuation artifact (*7*). In view of the growing need for noninvasive cardiac imaging, a perfusion tracer with a more favorable organ biodistribution and better image uniformity may have an important impact on CAD management.

PET provides a technology with the ability to perform nonuniform attenuation correction as well as better spatial and temporal resolution than SPECT. Better temporal resolution improves the counting rate and, consequently, image quality. To date, despite these important advantages, PET is rarely used to assess myocardial perfusion clinically. ^{15}O-Water and ^{13}N-ammonia are excellent PET perfusion tracers and may provide a good quantitative estimate of coronary blood flow (*8,9*). However, the use of ^{15}O-water and ^{13}N-ammonia has been limited to a small number of medical centers with an on-site cyclotron because of their

Received Dec. 8, 2006; revision accepted Feb. 22, 2007.
For correspondence or reprints contact: Igal Madar, PhD, JHOC 4230, 601 N. Caroline St., Baltimore MD 21287.
E-mail: imadar@jhmi.edu

short half-lives. ^{82}Rb, produced by generator, is the most frequently used PET perfusion tracer in the clinical setting (*10*). However, ^{82}Rb has a lower extraction fraction than ^{15}O-water and ^{13}N-ammonia, has less-than-optimal photon energy, is expensive, and its very short half-life (78 s) necessitates the introduction of relatively high doses, resulting in a high fraction of dead times and randoms and, consequently, noisy images (*11*). A PET perfusion agent labeled with a longer-life positron emitter, such as ^{18}F, may overcome some of these limitations. In addition, because of the smaller positron energy and, therefore, smaller propagation distance until annihilation, a ^{18}F-tagged agent would also have better spatial resolution than ^{82}Rb (*11*).

To address this need, we developed a series of ^{18}F-labeled phosphonium cations (*12*). To date, ^{18}F-fluorobenzyl triphenyl phosphonium (^{18}F-FBnTP) demonstrated the best imaging characteristics. Like the technetium complexes ^{99m}Tc-sestamibi and ^{99m}Tc-tetrofosmin, it targets mitochondria via a membrane potential-dependent mechanism (*13*). ^{18}F-FBnTP is a metabolically stable agent with minimal defluorination, demonstrating excellent characteristics as a cardiac imaging agent in healthy dogs, documented by dynamic PET (*14*). It has a fast and extensive accumulation and prolonged retention in the myocardium, a rapid decline of activity to very low values in the lungs and blood pool, and a liver uptake lower than heart activity. Importantly, ^{18}F-FBnTP demonstrated uniform distribution throughout the entire myocardium with a covariance of 6%–8% in the septum-to-lateral wall axis as well as the base-to-apex axis. The fast distribution kinetics of ^{18}F-FBnTP made high-contrast, uniform images possible by using short (10 min) scans, acquired early (5 min) after administration.

The objective of this study was to characterize the ability of ^{18}F-FBnTP to detect and assess the magnitude of coronary flow disparity and the size of the risk area in dogs with acute coronary artery stenosis of various degrees of severity. ^{18}F-FBnTP myocardial regional activity was measured ex vivo by direct tissue counting and in vivo by dynamic PET. ^{18}F-FBnTP myocardial regional uptake was compared ex vivo with that of ^{99m}Tc-tetrofosmin.

MATERIALS AND METHODS

Dog Preparation

Seventeen adult mongrel dogs of either sex, weighing 20–30 kg, were anesthetized with thiopental sodium (20 mg/kg), intubated, and ventilated on a respirator (Harvard Apparatus). Anesthesia was maintained by isoflurane (2.5%), administered by a Draeger anesthesia machine. When the animals were transported to or from the imaging laboratory, they were respirated with an Ambu-bag (NWMedical Solutions). The following vital signs were continuously monitored, recorded approximately every 15 min and maintained at physiologic level throughout the study: systolic blood pressure (BP), diastolic BP, heart rate, Spo_2 (oxygen saturation as measured by pulse oximetry), $Spco_2$ (carbon dioxide saturation as measured by pulse oximetry), respiratory rate and volume, temperature, and anesthesia level. Two femoral arteries, one femoral vein, the right jugular vein, and the right carotid artery were cannulated with 9-French sheaths. A 6-French pig-tailed catheter was placed, using fluoroscopic guidance, in the left ventricle by way of one of the femoral artery sheaths for the injection of radioactive microspheres. The other femoral artery sheath was used to collect blood for a microsphere reference blood-flow sample. The venous sheaths were used for tracer, drug, and fluid injections.

The left anterior descending (LAD) coronary artery or the left circumflex (LCx) coronary artery was dissected free 1–2 cm from origin, a cuff occluder was placed around the artery, and a Doppler ultrasonic flow probe was placed just proximal to the occluder. All procedures were approved by the Johns Hopkins Institutional Animal Care and Use Committee, and conformed to the American Heart Association Guidelines for the Use of Animals in Research.

Experimental Protocols

Protocol 1: Assessment of Perfusion Defect by Direct Tissue Counting. The experimental protocol is depicted in Figure 1A. During the baseline period, before stenosis was created, radioactive microspheres (MS1) were administered to measure baseline blood flow as described. Next, the coronary artery was partially occluded. Severity of occlusion was assessed by the magnitude of the reactive hyperemic (RH) response. The RH response of the occluded vessel was determined by snaring of the occluder for 10 s and then releasing the snare to produce a RH response to this transient vessel occlusion. Angiographic validation was not performed. To produce a "severe stenosis" the snare was adjusted to completely abolish the hyperemic response to this transient vessel occlusion, without affecting baseline flow. A "mild stenosis" was defined as an approximate 50% reduction in the RH response. After stenosis was established, a second set of microspheres (MS2) was administered. Next, adenosine infusion was begun at a rate of 0.14 mg/kg/min. At maximal adenosine effect (identified as maximal blood flow by the flow probe), 111 MBq (3 mCi) of ^{18}F-FBnTP were administered by intravenous bolus injection, simultaneously with a third set of microspheres (MS3). Ten minutes later, the stenotic vessel was occluded completely and Monastral blue dye (0.5 mL/kg) was injected into the left atrium to demarcate the area at risk (absence of blue staining). Dogs were euthanized by elevating the isoflurane anesthesia (10%) and dissecting the heart. The heart was sliced into five 1- to 1.5-cm-thick rings, which were prepared for γ-well counting as described.

Protocol 2: Assessment of Perfusion Defect by Dynamic PET and Direct Tissue Counting. Stenosis was established in the LAD ($n = 4$) or LCx ($n = 4$) coronary artery. The experimental protocol

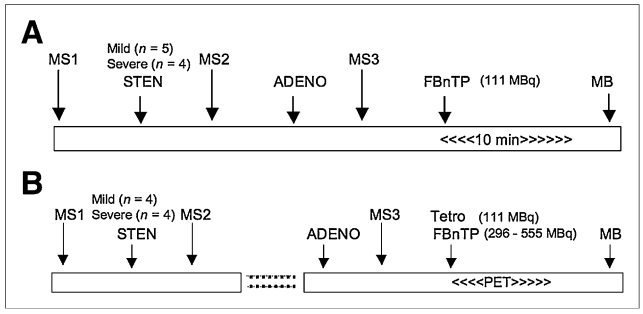

FIGURE 1. Experimental protocols. MS = microspheres; STEN = stenosis; ADENO = adenosine; MB = Monastral blue; Tetro = tetrofosmin.

is depicted in Figure 1B. After stenosis was established and MS1 and MS2 microspheres were administered, as described in protocol 1, the dogs were attached to a cradle in a prone position and transferred to the PET suite. The dogs were positioned on the scanner bed so that the heart was centered in the scanner field of view (FOV), aided by repeated 1-min transmission scans, using a ^{68}Ge/^{68}Ga source. PET images were acquired on a GE Healthcare Advance scanner (35 axial slices, 4.25-mm thick, 14.4-cm axial FOV). A 10-min transmission scan was performed for subsequent attenuation correction. Next, adenosine was administered at a rate of 0.25 mg/kg/min. At peak blood flow, a dynamic PET scan was started together with the simultaneous injection of microspheres into the left atrium and intravenous administration of a mixture of 296–555 MBq (8–15 mCi) ^{18}F-FBnTP and 111 MBq (3 mCi) ^{99m}Tc-tetrofosmin. Because of the shorter half-life, ^{18}F-FBnTP was given in a larger dose than ^{99m}Tc-tetrofosmin—to compensate for the radioactivity decay—taking place during the time interval between tracer injection and the γ-well counting. The scan duration was 5 s × 24, 60 s × 5, 120 s × 4, and 300 s × 9, for a total time 60 min. At completion of the imaging procedures, Monastral blue was injected and the heart was removed and sliced into 1- to 1.5-cm-thick rings, which were prepared for radioactivity counting as outlined below. The dosing of adenosine in protocol 2 was adopted from an experimental protocol of other laboratories (*16*) to allow comparison with results of the present study.

Image and Data Analysis

Image Processing. PET scans were corrected for radioactivity decay as well as for attenuation by using the acquired transmission scan. To prevent error due to misregistration of the transmission and emission scans, dogs were strapped to the scanner bed, anesthetized, and continuously monitored for possible movement. Image reconstruction was accomplished by filtered ordered-subset expectation maximization (OSEM, 2 iterations, 18 subsets) using a 26 × 26 cm FOV, 256 × 256-pixel matrix, and 2 × 2 × 4.25 mm voxel size. Reformatting oblique slices to vertical and horizontal long-axis and transverse short-axis images was performed on an Xeleris Functional Imaging workstation (GE Healthcare). Short-axis slices (4-mm^3 voxel) were used to generate polar maps. Circumferential activity profiles were generated by radial sampling of maximum values on short-axis images summed over a preselected postinjection time interval. Twenty-four sectors (15° each), beginning at the intersection of the right ventricular wall, the interventricular septum, and the left ventricular (LV) anterior wall, were placed in a counterclockwise direction on the short-axis slices from base to apex. Time–activity curves were generated using the region-of-interest (ROI) method. ROIs (4 × 4 mm) were positioned at the center of the LV wall on the short-axis images summed over the 30- to 60-min time interval. Four ROIs were placed on each quadrant; a single ROI was placed in the middle of the LV chamber. The ROI template was transferred to the serial images of the corresponding short-axis slice, and time–activity curves were generated. Image processing was performed using an Analyze package (Mayo Clinic Analyze; Mayo Clinic, Rochester, MN).

Quantification of Regional Myocardial Blood Flow with Microspheres, ^{18}F-FBnTP, and ^{99m}Tc-Tetrofosmin Activities. Measurements of regional coronary flow were obtained at preselected times by injecting microspheres into the LV, while simultaneously collecting reference blood from a femoral artery catheter. For each measurement, 2 million 15-μm spheres (Perkin Elmer Co.) labeled with ^{57}Co, ^{113}Sn, ^{103} Ru, ^{95}Nb, or ^{46}Sc were administered, while a reference blood sample was obtained from an aortic catheter, at a rate of 2.16 mL/min, for 130 s, starting 10 s before injection of the microspheres.

The Monastral blue–stained LV slices were photographed and traced on a plastic transparency to indicate slice borders and outline the risk and normal regions. Each ring was sectioned radially into multiple radial pieces, and each in turn was sectioned into epicardial and endocardial halves. The location of each transmural wedge was recorded on the transparency. This allowed, later on, correlation of the activity measured ex vivo and in vivo from overlapping regions in an accurate manner. Each piece was weighed and counted in a γ-counter for 10 min. ^{18}F activity was counted immediately after dissection; technetium activity was counted 24 h after dissection, and microsphere activities were counted 72 h thereafter. Tissue counts were corrected for decay, background, and isotope spillover. Transmural activity was calculated as the average of corresponding epicardial and endocardial samples. Coronary blood flow was calculated as previously described (*15*).

The ischemic-to-nonischemic (IS/NIS) activity ratio was calculated for the 3 midventricular rings. The representative activity of ^{18}F-FBnTP, ^{99m}Tc-tetrofosmin, and microspheres in the stenotic area was calculated as the mean activity counted in 2 successive transmural tissue samples, collected from the stenotic zone, and demonstrated the lowest microsphere flow at the time adenosine was injected. Similarly, the representative activity of the normal bed was calculated as the mean of 2 transmural tissue samples demonstrating the highest microsphere flow during adenosine injection.

Quantitation of the IS/NIS activity ratio on the ^{18}F-FBnTP PET images was obtained by selecting short-axis images visually corresponding to the basal aspect of the 3 midventricular anatomic slices, based on measuring the inner and outer ring diameters, and the anatomic indices, the RV−LV junctures, and the papillary muscle, which were easily visualized on short-axis PET images of all dogs. Monastral blue−stained myocardial tissue sections were about 1-cm thick. Because of the geometry of the ischemic zone, the size of the Monastral blue−negative area is not necessarily the same on the basal and the apical faces of individual slices. Therefore, matching of PET and tissue slices was accomplished while tissue slices were placed with their basal side facing up. Next, a histogram of the circumferential activity profile of the selected short-axis PET images was generated, using radial sampling, 24 sectors, 15° each. The mean value of sectors in regions, corresponding to the stenotic and normal regions on Monastral blue−stained slices, was computed.

Determination of Risk Area Size. Size of the risk area on individual Monastral blue−stained myocardial sections and coplanar short-axis PET images was calculated using digital planimetry (GTCO Digitizing Tablet) as a fraction of the total slice area. PET images and anatomic myocardial slices were matched as described.

Statistical Analysis

Differences between means within a group of dogs were assessed by repeated-measures ANOVA, and post hoc comparisons were made using the Scheffé test. Paired Student *t* tests with values of $P \leq 0.05$ were considered significant. Groups of dogs were compared by 1-way ANOVA. Linear regression analyses

TABLE 1
Hemodynamic Parameters

Parameter	Baseline	Stenosis	Adenosine
Heart rate (bpm)	117.6 ± 12.4	122.4 ± 13.1	109.2 ± 21.7
Systolic BP (mm Hg)	101.3 ± 10.4	98.1 ± 10.3	96.8 ± 11.1*
Diastolic BP (mm Hg)	74.0 ± 8.2	67.5 ± 7.4	63.4 ± 13.3*
Respiratory rate	10.8 ± 0.6	10.1 ± 1.2	11.5 ± 0.9
Respiratory volume	301.0 ± 27.4	291.6 ± 27.2	283.7 ± 32.6

*$P \geq 0.323$ vs. stenosis.
Values are mean ± SD.

were performed using Spearman linear regression. Statistical analysis was performed using a STATA package (StataCorp.).

RESULTS

Hemodynamics

Hemodynamics were monitored continuously and remained stable throughout the study (Table 1). There was no significant difference in hemodynamics measures between dogs in protocols 1 and 2; therefore, data were pooled.

Microsphere Blood Flow

Mean absolute transmural blood flow in the stenotic and normal beds before and after stenosis, as well as during administration of adenosine at a rate of 0.14 mg/kg/min (protocol 1) or 0.25 mg/kg/min (protocol 2), is shown in (Table 2). "Baseline" and "Stenosis" values represent data pooled from protocol 1 and 2 dogs.

Comparison Between ^{18}F-FBnTP and ^{99m}Tc-Tetrofosmin Activities

Figure 2 depicts the myocardial activities of ^{18}F-FBnTP and ^{99m}Tc-tetrofosmin, versus microsphere flow, in endocardial and epicardial samples from dogs with either severe or mild stenosis during adenosine vasodilation. Tracer activity is normalized to the mean activity in the normal bed. At low flow rates (<0.5 mL/g/min), ^{18}F-FBnTP approached zero values faster than ^{99m}Tc-tetrofosmin. The myocardial activity of both tracers plateaued as flow increased. However, the upslope of radioactivity in the range of flow rates ≥ 1.5 mL/g/min was greater for ^{18}F-FBnTP (0.075) than that for ^{99m}Tc-tetrofosmin (0.013).

The IS/NIS activity ratio was calculated for ^{18}F-FBnTP, ^{99m}Tc-tetrofosmin, and microsphere flow during adenosine infusion at 0.25 mg/mL/kg in the mild and severe stenosis groups (Fig. 3A). In both groups of dogs, the ^{18}F-FBnTP estimate of the flow defect (IS/NIS ratio: mild, 0.72 ± 0.08; severe, 0.42 ± 0.05) was significantly ($P \leq 0.03$) more accurate than that of ^{99m}Tc-tetrofosmin (mild, 0.93 ± 0.07; severe, 0.64 ± 0.08) but was significantly lower ($P < 0.05$) than the microsphere flow defect count ratio (mild, 0.43 ± 0.06; severe, 0.22 ± 0.04). Similar relationships were observed when adenosine was administered at the clinical dose (0.14 mg/kg/min) in the severe stenosis group (^{18}F-FBnTP, 0.63 ± 0.05; microsphere, 0.32 ± 0.04) and the mild stenosis group (^{18}F-FBnTP, 0.80 ± 0.03; microsphere, 0.59 ± 0.06) (Fig. 3B).

To further characterize the difference between ^{18}F-FBnTP and ^{99m}Tc-tetrofosmin, the IS/NIS ratios of ^{18}F-FBnTP and ^{99m}Tc-tetrofosmin, calculated for individual myocardial sections (3 sections per dog; 8 dogs), were correlated with the microsphere flow ratio during adenosine infusion (Fig. 3C). ^{18}F-FBnTP and ^{99m}Tc-tetrofosmin demonstrated a good linear correlation versus microsphere flow,

TABLE 2
Blood Flow Measured by Microspheres

Stenosis	Baseline	Stenosis	Adenosine	
			0.14 mg/kg/min	0.25 mg/kg/min
Severe				
Ischemic	0.97 ± 0.02	0.90 ± 0.049	1.10 ± 0.21*	0.69 ± 0.31*
Nonischemic	0.95 ± 0.02	1.03 ± 0.057	3.45 ± 0.47	3.18 ± 0.12
Mild				
Ischemic	1.09 ± 0.05	0.99 ± 0.043	1.42 ± 0.11*	1.52 ± 0.20*
Nonischemic	1.03 ± 0.03	1.07 ± 0.025	2.51 ± 0.43	3.01 ± 0.21

*$P < 0.03$ vs. stenosis.
Values are mL/g/min (mean ± SEM).

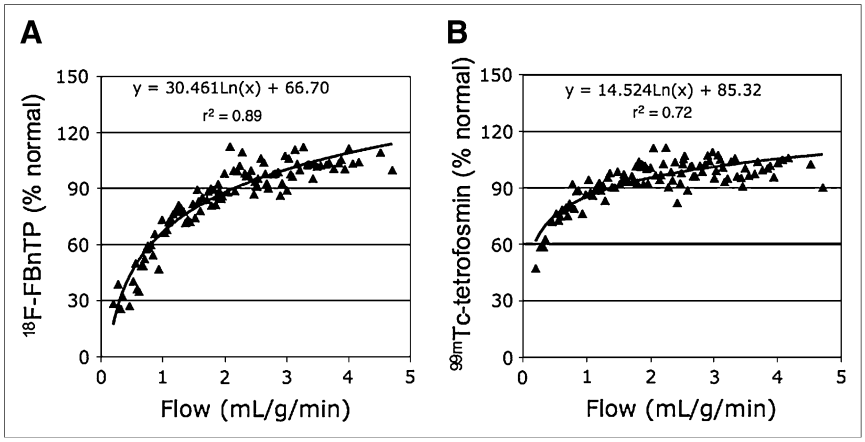

FIGURE 2. Normalized ^{18}F-FBnTP (A) and ^{99m}Tc-tetrofosmin (B) activities plotted as a function of microsphere flow during adenosine infusion from endocardial and epicardial samples of dogs with mild-to-severe stenosis. Both tracers overestimate and underestimate blood flow rates in the low and the high range, respectively, but ^{18}F-FBnTP contrast between low and high flow rates is greater than that of ^{99m}Tc-tetrofosmin. For the sake of visual clarity, data per dog were sorted according to microsphere flow, and each point represents the mean of 4 neighboring values.

with a similar slope (1.25 vs. 1.31, respectively). Because the regression lines were nearly parallel, the difference between the 2 tracers can be reliably estimated by the intercept, which was much smaller for ^{18}F-FBnTP than for ^{99m}Tc-tetrofosmin (0.14 vs. 0.38, respectively). This indicates that the flow defect contrast (IS/NIS) is 2.7 times greater for ^{18}F-FBnTP than that for ^{99m}Tc-tetrofosmin.

^{18}F-FBnTP PET In Vivo

The mean IS/NIS activity ratios calculated on PET short-axis images acquired at 30–60 min after injection from mildly and severely stenotic dogs were very close to those obtained by direct tissue counting (0.70 ± 0.04 and 0.46 ± 0.02, respectively; $P \geq 0.330$). Moreover, the IS/NIS activity ratio calculated from individual short-axis images by PET demonstrated a strong linear correlation with activity ratios of ^{18}F-FBnTP ($R^2 = 0.94$) as measured from corresponding regions on coplanar myocardial sections by γ-well counting (Fig. 4A). Similarly, high correlation ($R^2 = 0.79$) was found between the flow defect count ratio measured by PET and microspheres (Fig. 4B).

Examples of cardiac ^{18}F-FBnTP PET images acquired in dogs with mild LCx, moderate LAD, or severe LCx flow defect are presented in Figure 5. For comparison, polar maps obtained from a healthy dog are presented in the far left column. Qualitatively, defect severity can be identified

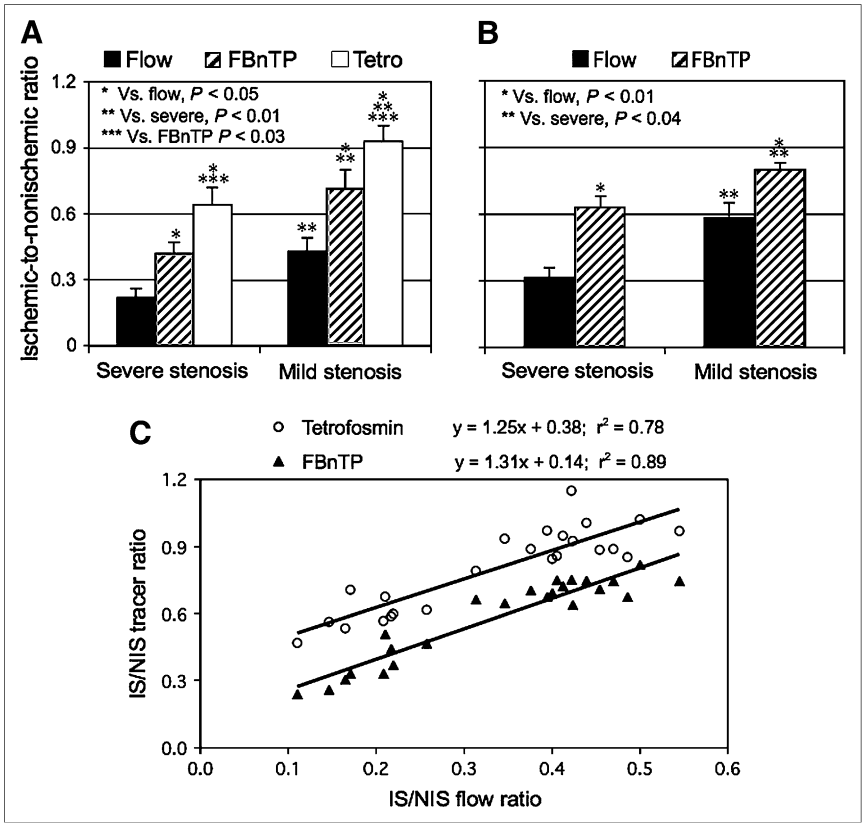

FIGURE 3. Mean IS/NIS activity ratio of microsphere flow and ^{18}F-FBnTP and ^{99m}Tc-tetrofosmin (Tetro) activities in dogs with severe and mild stenosis during adenosine administration at a rate of 0.25 mg/kg/min (A) and 0.14 mg/kg/min (B). ^{18}F-FBnTP provides a significantly more accurate estimate of defect severity than ^{99m}Tc-tetrofosmin, as compared with the microsphere flow defect count ratio. ^{18}F-FBnTP maintains a similar relationship with microsphere defect flow during administration of adenosine in clinical and supraclinical doses. (C) ^{18}F-FBnTP and ^{99m}Tc-tetrofosmin versus microsphere flow activities expressed as IS/NIS activity ratio calculated for individual myocardial sections (3 per dog) in dogs with various degrees of stenosis ($n = 8$). Flow defect contrast is 2.7 times greater for ^{18}F-FBnTP than that for ^{99m}Tc-tetrofosmin, as inferred from the curve intercepts (0.14 and 0.38, respectively).

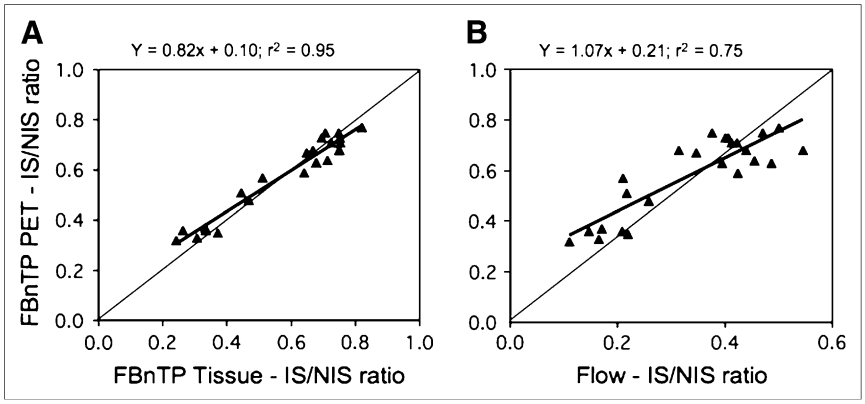

FIGURE 4. IS/NIS activity ratio calculated by PET is plotted against the IS/NIS calculated by well counting for ^{18}F-FBnTP (A) and microsphere flow (B) from coplanar myocardial sections (3 slices per dog; 8 dogs). In vivo estimate of flow defect using PET closely corresponds to tracer and flow activity counted directly in tissue.

by visual inspection of the short-axis images and polar maps. Quantitative values of the IS/NIS ratio were calculated from the circumferential activity profiles (bottom row) generated from the short-axis PET images (second row). The ^{18}F-FBnTP IS/NIS ratios obtained with PET in the mildly, moderately, and severely stenotic dogs were 0.74, 0.64 and 0.33 compared with 0.55, 0.45, and 0.16 measured by microspheres, respectively.

Detection and Imaging of Flow Defect Using Early, Short ^{18}F-FBnTP PET Scans

Defect contrast was measured on 10-min scans acquired 5 min postinjection and compared with that obtained on 30–60 min scans. Nearly identical IS/NIS activity ratios were obtained by the early, short vs. the delayed, prolonged scans (R^2 = 0.98, slope = 1). Figure 5 demonstrates the polar plots of 5–15 min and 30–60 min scans obtained in the mildly, moderately and severely stenotic dogs. The stenotic zone could be identified, and a distinction between severities of stenosis could be discerned with the same visual clarity on the short, early scan, as on the prolonged, delayed scan. The close similarity between the 5–15 and 30–60 min scans can be appreciated quantitatively by the overlap of circumferential activity profiles (Fig. 5, bottom row).

Size of Area at Risk by ^{18}F-FBnTP PET

In 7 of 8 dogs, the risk area was measured on coplanar PET images and Monastral blue–stained myocardial slices, using planimetry. In 1 dog, staining was too faint to accurately demarcate the boundaries of the risk area. Examples of stained myocardial rings and corresponding PET short-axis images are presented in Figure 5. A strong

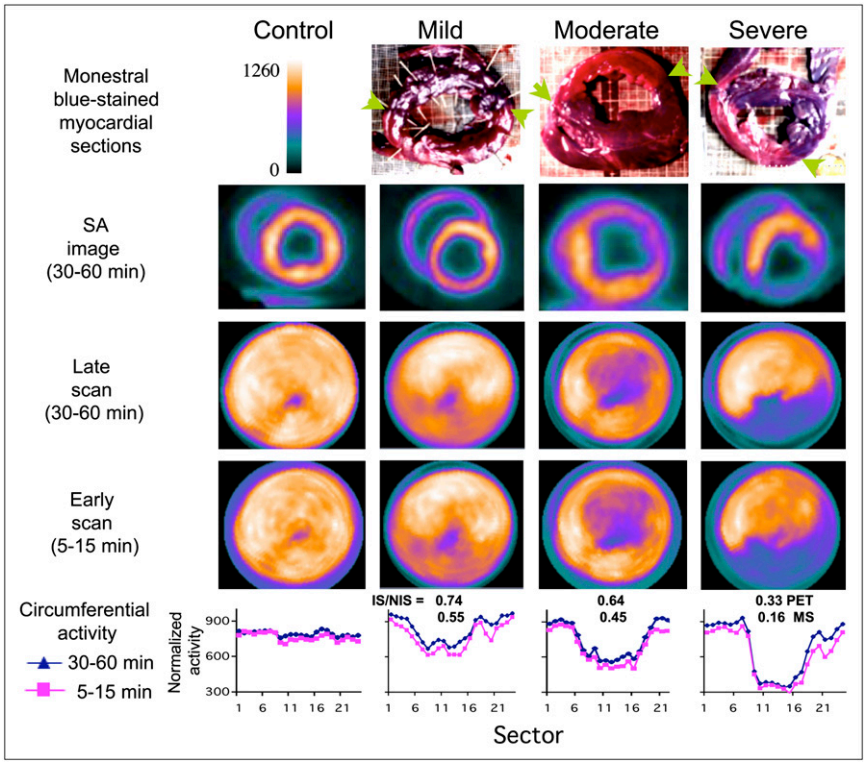

FIGURE 5. Examples of ^{18}F-FBnTP PET images acquired in dogs with mild LCx, moderate LAD, or severe LCx stenosis. For purposes of comparison, ^{18}F-FBnTP PET polar maps acquired in a healthy dog are presented in far left column. Monastral blue–stained anatomic slices, and 30- to 60-min coplanar ^{18}F-FBnTP PET short-axis (SA) images, as well as polar maps acquired over 30- to 60-min and 5- to 15-min time intervals, are presented. Ischemic zone on anatomic sections is of lighter color, its boundaries indicated by green arrows. Circumferential activity profile of short-axis images (second row), summed over 30- to 60-min and 5- to 15-min time intervals, is presented (bottom row). Activity profiles are normalized to the global mean per dog. Mean IS/NIS of ^{18}F-FBnTP (PET) and microsphere flow (MS), calculated for each dog, is presented in bottom row.

linear correlation ($R^2 = 0.72$) was found between the size of the risk area determined from PET and the Monastral blue−negative region, as measured in individual slices (7 dogs, 21 slices) (Fig. 6). Size of the risk area is expressed as the fraction of the total slice area. The mean risk size on PET was 16% lower than that measured on stained myocardial slices (0.31 ± 0.05, 0.37 ± 0.03, respectively).

^{18}F-FBnTP Uptake Kinetics

^{18}F-FBnTP kinetics in the stenotic and normal beds was characterized using dynamic PET. ^{18}F-FBnTP accumulation during the first 2 min was documented by 5-s scans. The time–activity curves generated on short-axis PET images demonstrated rapid accumulation and equilibration of ^{18}F-FBnTP in the stenotic and normal beds during adenosine vasodilation. Peak activity was obtained within 10–20 s after injection, and a near-plateau concentration 10–20 s thereafter, which was retained throughout the scanning time (up to 60 min). Time-to-peak activity was very consistent throughout myocardial segments within dogs, as well as between dogs. No significant difference in time-to-peak activity in the stenotic and normal zones was observed ($P > 0.136$). In all dogs, however, ^{18}F-FBnTP peak activity was significantly ($P < 0.0011$) lower in the stenotic zone (190.4 ± 26.1 Bq/cm^3/MBq) than that in the normal zone (395.5 ± 60.96 Bq/cm^3/MBq). Similar retention kinetics was observed in the stenotic and normal zones. Figure 7 depicts a representative example of ^{18}F-FBnTP time–activity profile in a mildly stenotic dog.

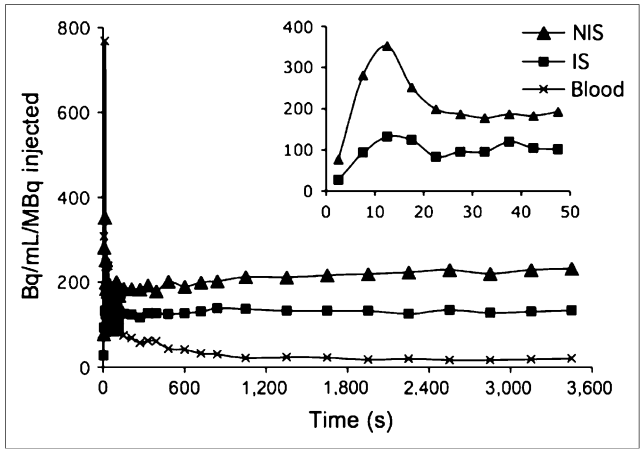

FIGURE 7. ^{18}F-FBnTP time–activity curves in stenotic and normal zones and LV chamber from dog with mild stenosis.

DISCUSSION

The objective of this study was to characterize, in vivo and ex vivo, the capacity of the PET compound ^{18}F-FBnTP to assess the flow defect severity and the size of the risk area, using microsphere blood flow and Monastral blue staining, respectively, as gold standards. ^{18}F-FBnTP myocardial uptake was directly compared with ^{99m}Tc-tetrofosmin, a clinically accepted perfusion agent. ^{99m}Tc-Tetrofosmin was selected as a reference tracer because both tracers are sequestered by cells via a similar membrane potential-dependent mechanism (*13,16*) and retained in the myocardium for a prolonged time (*14,17*). Because of better imaging properties, ^{99m}Tc-tetrofosmin and ^{99m}Tc-sestamibi are more frequently used in clinical MPI studies than ^{201}Tl (*18*). Therefore, ^{99m}Tc-tetrofosmin affords an appropriate candidate for assessing the potential clinical utility of ^{18}F-FBnTP. In the present study, ^{18}F-FBnTP was compared with ^{99m}Tc-tetrofosmin under ex vivo conditions. Taking into consideration the better spatial and temporal resolution of PET compared with SPECT, most likely, the better performance of ^{18}F-FBnTP observed ex vivo will be retained during PET.

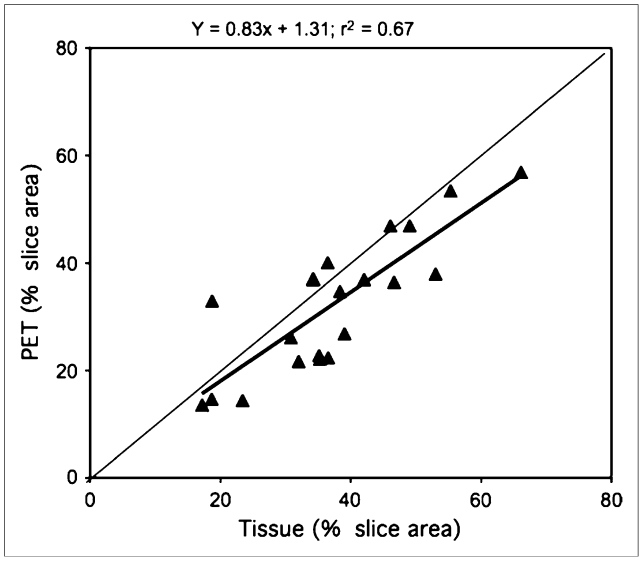

FIGURE 6. Defect size measured on PET images and Monastral blue−stained myocardial rings (7 dogs, 21 rings). Values represent extent of stenotic zone as a fraction of total slice area.

Assessment of Flow Disparity

The data demonstrated in Figure 2 show both ^{18}F-FBnTP and ^{99m}Tc-tetrofosmin overestimated flow in the low range and underestimated flow in the high range but ^{18}F-FBnTP agreed more closely with microsphere flow than ^{99m}Tc-tetrofosmin. At flow rates < 0.5 mL/min/g, ^{18}F-FBnTP approached zero values faster than ^{99m}Tc-tetrofosmin. At high flow rates ≥ 1.5 mL/min/g, ^{99m}Tc-tetrofosmin reached a plateau concentration, whereas the amount of ^{18}F-FBnTP taken up by the myocardium continued to rise at a significantly greater rate. The ^{18}F-FBnTP upslope was 0.075 compared with 0.013 for ^{99m}Tc-tetrofosmin. Other dog studies report that ^{99m}Tc-tetrofosmin myocardial accumulation reaches a plateau at flow rates > 1.5–2 mL/min/g (*15,17–21*). The greater upslope at high flow rates indicates greater myocardial extraction, as demonstrated for other perfusion tracers (*15*). The behavior of ^{18}F-FBnTP is more desirable for stress–rest studies because it increases the

contrast of flow defect. However, further studies are needed to directly quantify the ^{18}F-FBnTP extraction fraction in the myocardium, using first-pass models (*9,15,22,23*).

A more detailed comparative analysis of ^{18}F-FBnTP and ^{99m}Tc-tetrofosmin flow-dependent uptake was obtained by examining the relationships of the IS/NIS activity ratios calculated for individual myocardial sections. The IS/NIS ratio of both tracers correlated linearly with the flow defect count ratio and resulted in near-parallel linear regression curves for ^{18}F-FBnTP and ^{99m}Tc-tetrofosmin. The difference in the capacity to distinguish flow disparity can be assessed by the intercept of the linear regressions (Fig. 3C), which was smaller for ^{18}F-FBnTP than for ^{99m}Tc-tetrofosmin (0.14 vs. 0.38, respectively). This finding suggests that the contrast between the ischemic and normal beds is nearly 2.7 times greater for ^{18}F-FBnTP than for ^{99m}Tc-tetrofosmin and that this difference is consistent, regardless of the severity of stenosis. The better distinction between ischemic and normal beds is in line with the finding that ^{18}F-FBnTP is more responsive than ^{99m}Tc-tetrofosmin to alterations in blood flow rate in the low and high range as well.

Several factors may underlie the better extraction of ^{18}F-FBnTP compared with ^{99m}Tc-tetrofosmin. Uptake and retention mechanisms are important determinants of the net accumulation of a tracer in the myocardium. However, these factors may have little contribution, as both ^{18}F-FBnTP and ^{99m}Tc-tetrofosmin accumulate in cells in a membrane potential-dependent manner (*13,16*), as well as demonstrate prolonged retention in the myocardium (*14,17*). The rate of diffusion through membranes of the capillary wall endothelial cells, as well as the parenchymal cells is key to the capacity of a tracer to follow high flow rates, as described by the Gosselin and Stibitz model (*24*). In vitro kinetics assays suggest that ^{18}F-FBnTP permeates cellular membranes faster than ^{99m}Tc-tetrofosmin. In isolated ventricular myocytes, the time to reach a plateau concentration was 30 min for ^{18}F-FBnTP (*14*) compared with 60 min for ^{99m}Tc-tetrofosmin (*16*). The overall molecular size and geometry, as well as the lipophilicity of these 2 agents are clearly different, and these factors must impact on the transmembrane exchange process. The molecular size of ^{99m}Tc-tetrofosmin, a diphosphine complex, is much greater than that of ^{18}F-FBnTP, and this probably plays a major role in limiting its passage across the capillary barrier. Lipophilic cationic compounds cross the lipid bilayer barrier by passive diffusion, which is governed by attractive hydrophobic and repulsive electrostatic forces (*24*). The attractive hydrophobic effect increases with increasing the cation solvent-accessible surface area (*25*), which is expected to be larger for ^{18}F-FBnTP because of its much smaller molecular size than ^{99m}Tc-tetrofosmin.

Potential Clinical Implications

The potential clinical utility of ^{18}F-FBnTP was evaluated by PET in dogs with varying degrees of stenosis. The accuracy of quantifying the flow defect by PET was assessed by comparing the IS/NIS activity ratio with that calculated by direct tissue counting. The mean ^{18}F-FBnTP IS/NIS activity ratio measured from PET in the mild and severe stenosis groups was nearly identical to that obtained by well counting. Similarly, the ^{18}F-FBnTP PET IS/NIS ratio, calculated for individual myocardial short-axis images, demonstrated a direct strong linear correlation (R^2 = 0.94), overlapping the line of identity, with the tissue activity ratio measured ex vivo. This finding suggests that the better performance of ^{18}F-FBnTP compared with ^{99m}Tc-tetrofosmin, observed ex vivo, will be expressed in vivo as well using cardiac PET.

The size of the risk area measured on individual PET images was very close to that measured on Monastral blue–stained coplanar cardiac sections. The mean risk area on PET was 84% of the true extent as measured on the stained sections. The ^{18}F-FBnTP underestimation of risk area is much smaller than that reported for technetium complexes. SPECT studies in 7 dogs with partial coronary occlusion show that the defect size on ^{99m}Tc-sestamibi images was only a fraction (37% ± 30%) of that measured by ^{201}Tl scans (*26*). Similar observations were obtained in clinical studies (*27–30*). The better efficacy of ^{201}Tl may be attributed to the better extraction fraction, compared with the technetium complexes (*21,25,27*). This suggests that in addition to methodologic factors—such as the PET scanner better resolution and attenuation correction—the relatively accurate delineation of risk area observed in the current study reflects the capability of ^{18}F-FBnTP to follow coronary blood flow over a wide range of rates better than ^{99m}Tc-tetrofosmin.

Scatter of photons from extracardiac structures (e.g., liver) introduces artifacts that may mask the detection of perfusion defects mainly in the inferior LV wall. Another factor, which may affect the defect contrast on noninvasive imaging scans, is the background activity residing in the lung parenchyma. Sinusas et al. (*18*) reported that in dogs the ^{99m}Tc-tetrofosmin LV wall-to-liver and LV wall-to-lung uptake ratios, at 30 min after injection, are 1:1.7 and 2:1, respectively, compared with 1.2:1 and 12:1, found for ^{18}F-FBnTP in the same species (*14*). In addition, ^{18}F-FBnTP PET showed a highly uniform distribution of activity throughout the entire myocardium, including the inferoapical aspect, with covariance in the short and longitudinal axes of only 6%–8% (*14*). This finding suggests that regional decreases of ^{18}F-FBnTP myocardial activity as small as 8% can be detected with confidence $>1\sigma$ (68%) on PET images. The excellent image uniformity and contrast, combined with the better perfusion characteristics, as well as the scanner methodologic advantages, suggest that ^{18}F-FBnTP PET may resolve small flow defects undetected by ^{99m}Tc-tetrofosmin SPECT scans.

Clinical perfusion studies indicated that the SPECT sensitivity rate is not uniform throughout the entire myocardium. In a study of 113 patients with significant CAD, ^{99m}Tc-methoxyisobutylisonitrile SPECT sensitivity for recognizing disease in the LAD was 80% but it dropped

to 70% and 63% in the LCx and right coronary artery, respectively (*31*). More than other cardiac territories, the inferior wall is susceptible to attenuation artifacts and photon scatter from the liver (*32,33*). In the present study, in protocol 2, we occluded the LCx in 4 dogs and the LAD in 4 dogs. We did not find differences in detecting and assessing the severity of stenosis in these 2 groups of dogs, as compared with microsphere flow. In 3 dogs, the risk area was localized in the inferior wall (e.g., the dogs with mild and severe stenosis in Fig. 5). This suggests the potential of ^{18}F-FBnTP PET to identify the flow defect with same high accuracy throughout the myocardium.

Dynamic PET showed that ^{18}F-FBnTP reaches equilibrium concentrations in the myocardium within $<$1 min. The rapid distribution kinetics allowed acquiring images of high diagnostic quality using early, short (5–15 min) scans. The same defect contrast was obtained on 5- to 15-min and 30- to 60-min scans. The rapid kinetics combined with the favorable organ distribution and the fast clearance of extracardiac activity suggests that, with ^{18}F-FBnTP PET technology, perfusion studies can be performed shortly after injection. This may obviate the waiting period (1–2 h) recommended for SPECT studies, which is required for clearance of extracardiac activity.

In the present study, the performance of ^{18}F-FBnTP as a perfusion tracer was assessed in an acute model of ischemia, in which myocardial viability is intact. However, in a patient with chronic ischemia, myocardial viability might be affected as well, either reversibly (e.g., stunning) or irreversibly (e.g., infarct). The mitochondrial membrane potential ($\triangle\psi_m$) is the driving force of ^{18}F-FBnTP cellular uptake. $\triangle\psi_m$ is a sensitive measure of mitochondrial bioenergetics (*34*) and, hence, tissue viability. Therefore, alterations in myocardial viability are expected to affect the cellular uptake of the voltage sensor and thereby interfere with the detection of coronary blood flow abnormalities. However, SPECT studies using the $\triangle\psi_m$-targeted ^{99m}Tc-sestamibi suggest that imaging of resting myocardial blood flow and flow reserve is an effective approach for differentiating contractile dysfunction associated with flow abnormalities in the presence and absence of persistent or irreversible myocardial injuries (*1,2*). Further studies of chronic models of ischemia are required to characterize ^{18}F-FBnTP capacity to distinguish between blood flow and viability defects.

CONCLUSION

^{18}F-FBnTP demonstrated several characteristics, which are important for a successful MPI agent. (a) ^{18}F-FBnTP estimates of flow disparity, during adenosine-induced hyperemia, allow not only categoric distinction between mild and severe stenosis, but also a quantitative stratification of the magnitude and extent of flow defect over a wide spectrum of stenosis severity, significantly more accurate than ^{99m}Tc-tetrofosmin. (b) The ^{18}F-FBnTP PET defect contrast was very close to that measured by direct tissue counting ($r^2 = 0.95$, slope = 0.82). In view of the superior methodology of PET compared with SPECT, the better ex vivo performance of ^{18}F-FBnTP as the perfusion tracer, relative to ^{99m}Tc-tetrofosmin, will be enhanced in clinical MPI studies. (c) ^{18}F-FBnTP PET affords a relatively accurate measure of the extent/size of the flow defect. (d) The fast kinetics of ^{18}F-FBnTP allows one to obtain the high-contrast flow defect by a short, early PET scan. (e) The highly uniform distribution allows one to detect flow defects with the same accuracy regardless of the segmental localization. (f) The relatively longer half-life of ^{18}F may resolve some of the disadvantages of PET perfusion tracers, currently available in the clinical setting (^{82}Rb, ^{15}O, $^{13}NH_3$), and thus afford better exploitation of the superior imaging characteristics of the PET scanner as well as promote the role of PET in cardiac perfusion studies. These characteristics suggest that ^{18}F-FBnTP PET technology may provide a means for resolving small-magnitude flow defects not seen by SPECT studies, with the same high diagnostic accuracy throughout the entire myocardium, using a more efficient imaging protocol with better patient throughput.

ACKNOWLEDGMENT

This study was supported in part by a research grant from Nihon Mediphysics. We are grateful to Dr. Masroor Abro for technical assistance and Mr. David Clauth for performing the PET imaging.

REFERENCES

1. Beller GA. Prognostic applications of myocardial perfusion imaging: exercise stress. In: Zaret BL, Beller GA, eds. *Clinical Nuclear Cardiology.* 3rd ed. 2005:255–264.
2. Klocke FJ, Baird MG, Lorell BH, et al. ACC/AHA/ASNC guidelines for the clinical use of cardiac radionuclide imaging: executive summary—a report of the American College of Cardiology/American Heart Association Task Force on Practice Guidelines (ACC/AHA/ASNC Committee to Revise the 1995 Guidelines for the Clinical Use of Cardiac Radionuclide Imaging). *Circulation.* 2003; 108:1404–1418.
3. Heller EN, DeMan P, Liu YH, et al. Extracardiac activity complicates quantitative cardiac SPECT imaging using a simultaneous transmission-emission approach. *J Nucl Med.* 1997;38:1882–1890.
4. Higley B, Smith FW, Smith T, et al. Technetium-99m-1,2-bis[bis(2-ethoxyethyl)-phosphino]ethane: human biodistribution, dosimetry and safety of a new myocardial perfusion imaging agent. *J Nucl Med.* 1993;34:30–38.
5. Baghdasarian SB, Heller GV. The role of myocardial perfusion imaging in the diagnosis of patients with coronary artery disease: developments over the past year. *Curr Opin Cardiol.* 2005;20:369–374.
6. O'Connor MK, Kemp B, Anstett F, et al. A multicenter evaluation of commercial attenuation compensation techniques in cardiac SPECT using phantom models. *J Nucl Cardiol.* 2002;9:361–376.
7. Go V, Bhatt MR, Hendel RC. The diagnostic and prognostic value of ECG-gated SPECT myocardial perfusion imaging. *J Nucl Med.* 2004;45:912–921.
8. Bol A, Melin JA, Vanoverschelde JL, et al. Direct comparison of [^{13}N]ammonia and [^{15}O]water estimates of perfusion with quantification of regional myocardial blood flow by microspheres. *Circulation.* 1993;87:512–525.
9. Schelbert HR, Phelps ME, Huang SC, et al. N-13 ammonia as an indicator of myocardial blood flow. *Circulation.* 1981;63:1259–1272.
10. Schwaiger M, Muzik O. Assessment of myocardial perfusion by positron emission tomography. *Am J Cardiol.* 1991;67:35D–43D.
11. Machac J. Cardiac positron emission tomography imaging. *Semin Nucl Med.* 2005;35:17–36.
12. Ravert HT, Madar I, Dannals RF. Radiosynthesis of 3-[^{18}F]-fluoropropyl and 4-[^{18}F]-fluorobenzyl triarylphosphonium ions. *J Labelled Compds Radiopharm.* 2004;47:469–476.

13. Madar I, Ravert HT, Nelkin B, et al. Physiochemical characteristics and uptake kinetics of the voltage indicator [F-18]phosphonium cations [abstract]. *J Nucl Med.* 2003;44(suppl):14P.
14. Madar I, Ravert RT, Du Y, et al. Characterization of uptake of the new PET imaging compound [^{18}F]fluorobenzyl triphenyl phosphonium in dog myocardium. *J Nucl Med.* 2006;47:1359–1366.
15. Glover DK, Ruiz M, Yang JY, Smith WH, Watson DD, Beller GA. Myocardial ^{99m}Tc-tetrofosmin uptake during adenosine-induced vasodilatation with either a critical or mild coronary stenosis: comparison with ^{201}Tl and regional myocardial blood flow. *Circulation.* 1997;96:2332–2338.
16. Melin JA, Becker LC. Quantitative relationship between global left ventricular thallium uptake and blood flow: effects of propranolol, ouabain, dipyridamole, and coronary artery occlusion. *J Nucl Med.* 1986;27: 641–652.
17. Platts EA, North TL, Pickett RD, Kelly JD. Mechanism of uptake of technetium-tetrofosmin. I. uptake into isolated adult rat ventricular myocytes and subcellular localization. *J Nucl Cardiol.* 1995;2:317–332.
18. Sinusas AJ, Shi Q, Saltzberg MT, et al. Technetium-99m-tetrofosmin to assess myocardial blood flow: experimental validation in an intact canine model of ischemia. *J Nucl Med.* 1994;35:664–671.
19. Meleca MJ, McGoron AJ, Gerson MC, et al. Flow versus uptake comparisons of thallium-201 with technetium-99m perfusion tracers in a canine model of myocardial ischemia. *J Nucl Med.* 1997;38:1847–1856.
20. Canby RC, Silber S, Pohost GM. Relations of the myocardial imaging agents ^{99m}Tc-MIBI and ^{201}T1 to myocardial blood flow in a canine model of myocardial ischemic insult. *Circulation.* 1990;81:289–296.
21. Takahashi N, Reinhardt CP, Marcel R, Leppo JA. Myocardial uptake of ^{99m}Tc-tetrofosmin, sestamibi, and ^{201}Tl in a model of acute coronary reperfusion. *Circulation.* 1996;94:2605–2613.
22. Rosenbaum AF, McGoron AJ, Millard RW, et al. Uptake of seven myocardial tracers during increased myocardial blood flow by dobutamine infusion. *Invest Radiol.* 1999;34:91–98.
23. Herrero P, Markham J, Shelton ME, Weinheimer CJ, Bergmann SR. Noninvasive quantification of regional myocardial perfusion with rubidium-82 and positron emission tomography: exploration of a mathematical model. *Circulation.* 1990; 82:1377–1386.
24. Gosselin RE, Stibitz GR. Rates of solute absorption from tissue depots: theoretical considerations. *Pflugers Arch.* 1970;318:85–98.
25. Ross MF, Kelso GF, Blaikie FH, et al. Lipophilic triphenylphosphonium cations as tools in mitochondrial bioenergetics and free radical biology. *Biochemistry (Mosc).* 2005;70:222–230.
26. Honig BH, Hubbell WL, Flewelling RF. Electrostatic interactions in membranes and proteins. *Annu Rev Biophys Biophys Chem.* 1986;15:163–193.
27. Leon AR, Eisner RL, Martin SE. Comparison of single-photon emission computed tomographic (SPECT) myocardial perfusion imaging with thallium-201 and technetium-99m sestamibi in dogs. *J Am Coll Cardiol.* 1992;20:1612–1625.
28. Acampa W, Cuocolo A, Sullo P, et al. Direct comparison of technetium 99m-sestamibi and technetium 99m-tetrofosmin cardiac single photon emission computed tomography in patients with coronary artery disease. *J Nucl Cardiol.* 1998;5:265–274.
29. Soman P, Taillefer R, de Puey EG, Udelson JE, Lahiri A. Enhanced detection of reversible perfusion defects by Tc-99m-sestamibi compared to Tc-99m-tetrofosmin during vasodilator stress SPECT imaging in mild-to-moderate coronary artery disease. *J Am Coll Cardiol.* 2001;37:458–462.
30. Tamaki N, Takahashi N, Kawamoto M, et al. Myocardial tomography using technetium-99m-tetrofosmin to evaluate coronary artery disease. *J Nucl Med.* 1994;35:594–600.
31. Kapur A, Latus KA, Davies G, et al. A comparison of three radionuclide myocardial perfusion tracers in clinical practice: the ROBUST study. *Eur J Nucl Med Mol Imaging.* 2002;29:1608–1616.
32. Elhendy A, Sozzi FB, van Domburg RT, et al. Accuracy of exercise stress technetium 99m sestamibi SPECT imaging in the evaluation of the extent and location of coronary artery disease in patients with an earlier myocardial infarction. *J Nucl Cardiol.* 2000;7:432–438.
33. Hayes SW, De Lorenzo A, Hachamovitch R, et al. Prognostic implications of combined prone and supine acquisitions in patients with equivocal or abnormal supine myocardial perfusion SPECT. *J Nucl Med.* 2003;44:1633–1640.
34. Green DR, Kroemer G. The pathophysiology of mitochondrial cell death. *Science.* 2004;305:626–629.